Initiation and growth of a single pit on 316L stainless steel: Influence of SO42– and ClO4– anions

Nizar Aouina, F. Balbaud-Célérier, François Huet, Suzanne Joiret, Hubert Perrot, Fabien Rouillard, Vincent Vivier

Initiation and growth of a single pit on 316L stainless steel: Influence of SO_4^{2-} and ClO_4^- anions

N. Aouina[a,b], F. Balbaud-Célérier[c], F. Huet[a,b], S. Joiret[a,b], H. Perrot[a,b],

F. Rouillard[c,*], V. Vivier[a,b,*]

[a] *CNRS, UPR15, Laboratoire Interfaces et Systèmes Electrochimiques, F-75005 Paris, France*

[b] *UPMC Université P. et M. Curie, UPR15, LISE, 4 place Jussieu, F-75005 Paris, France*

[c] *CEA, DEN, DPC, SCCME, Laboratoire d'Etude de la Corrosion Non Aqueuse, F-91191 Gif-sur-Yvette, France*

Abstract

In this paper, an ion micro dispenser (IMD) was used to initiate a single pit by generating chloride anions above a 316L stainless steel electrode in either H_2SO_4 or $HClO_4$ electrolyte. The current variations with respect to time provided an unambiguous characterization of the single pit evolution. Different pit shapes were observed depending on both the nature of the electrolyte and potential applied to the electrode. Substituting SO_4^{2-} for ClO_4^- gave smaller (in diameter) but deeper pits at the early stage of pitting. However, when using a different setup that allows the sustaining of the pit propagation with a continuous supply of Cl^-, the deeper pits were observed in $HClO_4$ rather than H_2SO_4. The formation of an iron sulphate salt film at the bottom of the pit by precipitation of dissolution products in H_2SO_4 slowed down the corrosion rate. At high potentials, the repassivation mechanism outweighed the metal dissolution in the ClO_4^- solution containing solution.

Keywords: *pitting corrosion; pit propagation; ion micro dispenser; passivity breakdown*

[*]Corresponding authors.
V. Vivier Tel.: +33-1-44274158; fax: 33-1-44274074
E-mail address: vincent.vivier@upmc.fr
F. Rouillard Tel.: +33-1-69081614; fax: 33-1-69081586
E-mail address: fabien.rouillard@cea.fr

1. Introduction

It is well established that pitting corrosion on stainless steel (SS) occurs as a consequence of aggressive anions breaking through passivity and leading to the formation of a confined electrochemical micro-cell in which the attacked surface acts as an anode whereas the surrounding area acts as a cathode. Most of the formed pits behave as metastable events since they passivate within a few seconds after initiation. Only pits having a stability product $x.i$ (where x is the pit depth and i is the pit current density) larger than the critical value of 0.32 ± 0.2 A·m^{-1} in 1 M NaCl + 0.1 M H$_2$SO$_4$ solution propagate inside the material [1-3]. Electrochemical techniques such as electrochemical impedance spectroscopy (EIS) and cyclic voltammetry provide valuable information about the global properties of the metal/liquid interface and the generalized corrosion activity, but data interpretation is very complex because off the random nature of the pitting. To overcome this problem, some authors have worked on the development of a single pit, which allows a direct correlation between the measured data and the observed event. For instance, Alkire and Wong [4] developed a method for the initiation of a single pit on SS by masking all the surface with a thick photoresist coating except a domain of 100 μm in diameter left bare for the pit initiation when exposed to a chloride containing solution. The as-obtained pits were dish shaped with a depth-to-radius ratio close to 0.5. Maier and Frankel [5] have used a MgCl$_2$ droplet to initiate single pits on the surface a 304 SS. The effects of the drop size and concentration on the incubation time were studied and a mechanism for pit initiation and growth was proposed. Fushimi et al. [6, 7] used a silver/silver-chloride microelectrode to locally release chloride ions on iron in deaerated pH 6.5 borate solution. A 100 μm in diameter single pit grew solely when high potentials were applied to the iron sample. In a previous work [8], the same method was used to initiate a single pit on SS in sulphate acid media. Regardless the substrate potential, all the single pits remained active only for few minutes. In order to sustain the pit activity, Aouina et

2

al. substituted the Ag/AgCl probe by a glass micrcapillary in which chloride ions were injected at will from a syringe pump [9].

Laycock and White [10] [7] performed simulations of single propagating pits in stainless steel that reproduced major experimentally observed characteristics of pitting e.g. the pit evolution toward dish-shaped morphologies, development of a lacy cover and the spontaneous repassivation of metastable pits. In addition, the use of in situ microprobe X-ray fluorescence [11,12] and synchrotron X-ray diffraction [13] on lead-in-pencil electrodes showed that the salt film formed over dissolving 316L SS in acidic media was essentially composed of $FeCl_2$ beside little nickel and chromium.

Pitting factors such as the incubation time, the initiation site, the pit development as well as the shape of the final pit, are still hardly predictable. To shed light on the pitting behaviour, researchers have focused their attention on the most important parameters controlling the pit evolution, namely the chloride ion concentration, the solution pH, the temperature, and the polarization potential. Less attention has, however, been paid to the role played by non-aggressive anions in the pitting corrosion mechanism [15-21]. Most of the works mainly rely on potentiodynamic methods to measure the pitting potential as a function of either the nature of the non-aggressive anions or their concentration. In successive studies of various grades of SS, Leckie and Uhlig [15], Man and Gabe [16], and Zuo et al. [17] have shown that the pitting potential shifts toward nobler values when adding either OH^-, NO_3^-, SO_4^{2-}, ClO_4^-, CO_3^{2-}, PO_4^{3-} or CrO_4^{2-} anions into chloride ion containing solutions. The main conclusion is that non-aggressive anions act as pitting inhibitors due to their competitive adsorption with Cl^- on the SS surface. Leckie and Uhlig [15] reported that, for chloride ion concentration larger than 0.1M, the efficiency of pitting inhibition of 304 SS decreases in the order $OH^- > NO_3^- > SO_4^{2-} > ClO_4^-$. However, for low concentration of Cl^-, the inhibition effect of ClO_4^- outmatches that of SO_4^{2-}, as reported by Rosenfeld and Maximtschuk [22], suggesting the

involvement of additional factors in the adsorption mechanism. Among studies relating the anion effects to localised corrosion, particular attention has been paid to SO_4^{2-} ion [3, 23-26]. While most of the authors emphasized the competitive adsorption of SO_4^{2-} with Cl^-, which inhibits pitting [17, 23], others have reported that SO_4^{2-} could play an active role in the metal dissolution mechanism in certain environments [3, 26, 27]. According to Alkire and Wong [26], the formation of a $FeSO_4$ salt film was obtained at the bottom of pits on 304 SS in 1 N H_2SO_4 and 0.1 N NaCl at 0.6 V versus a saturated calomel electrode (SCE), instead of the iron-chloride complex ($FeCl_2$) usually described in the literature. These results are consistent with our previous work in which the formation of a $FeSO_4$, precipitating with chromium oxide (Cr_2O_3), was observed inside a pit formed on 316L SS in 0.5 M H_2SO_4 solution [8]. Pickering and Frankenthal [28, 29] have investigated the localized corrosion behaviour of iron as well as three different grades of steel (304 SS, Fe-20Cr alloy, and Fe-18Cr-8Ni alloy) in numerous electrolytes under potentiostatic polarization and under natural corrosion conditions. Their observations of pits, including those obtained in chloride-containing acidic media, show that the pit shape and morphology depend on both the nature of the initiation site and the solution composition. For instance, in the presence of SO_4^{2-}, pits grow hemispherically and the pit bottom seems to be polished due to the formation of a rate-limiting salt layer. Laitinen [30] investigated the effects of sulphate, thiosulphate, and chloride ions on the pitting behaviour of 304L SS at pH 3 and 5, and temperatures 55°C and 65°C. Apart from the highlighted sulphate inhibitive effect, increasing the amount of sulphate from 0 to 300 mg/L, led to larger pits (from 150 to 500 μm in diameter). After the thiosulphate addition, the deep empty pits formed in chloride and sulphate-containing solutions became opened pits, larger, and with oxides, as well as sulphur black deposits, inside. However, how chloride ions damage the material and how sulphate and thiosulphate intervene was not clear.

The present paper is aimed at establishing a deeper understanding of the role of non-aggressive ions in the pitting mechanism on 316 L SS. To overcome the random nature of pitting, the influence of sulphate and perchlorate anions on the initiation and propagation of pits on 316L SS has been investigated on single pits owing to two experimental approaches used in previous papers to form a single pit on iron [31-33] or SS electrodes [9].

2. Experimental part

2.1. Experimental setup and electrode preparation

All electrochemical investigations were performed using a scanning electrochemical microscope (SECM), which allows various types of corrosion processes to be investigated [34-40]. Pits were generated using a modified SECM setup including a 3-axis positioning system (VP-25XA, Newport) driven by a motion encoder (ESP300, Newport) allowing a spatial resolution of 100 nm in the three directions [8]. The electrochemical measurements were carried out with a lab-made bipotentiostat coupled to a low-noise current-to-voltage converter (Femto DLPCA200, BFI Optilas) with an adjustable gain (10^3–10^{11} V/A).

Two different approaches were developed to study the formation and the propagation of a single pit. In the first one (setup I), an Ag/AgCl electrode was used as a tank of chloride ions [33, 41]. Silver chloride was deposited on the tip of a 500 μm diameter silver wire insulated on its lateral surface with a cataphoretic paint and sealed into a 1 mm diameter glass capillary using an epoxy resin. This formed a reservoir of chloride ions that could be released at any defined location above the SS electrode by reduction of the deposit (it should be mentioned that changing the size , i.e. the diameter of the Ag wire, allows the total amount of Cl⁻ ions available for generating a pit to be also controlled). Prior to each AgCl deposit, the microelectrode was polished with SiC papers up to 4000 grade and rinsed in water under sonication. The AgCl layer was formed by anodizing the Ag microelectrode at a potential of

0.4 V/SCE in a 2 M KCl solution until the electrical charge exchanged, Q_{AgCl}, was about 15 mC (*vide infra*, some experiments were performed with other amounts of AgCl). The substrate was a 316L SS disk of 1.5 mm in diameter (S = 0.018 cm^2). Its dimension was small enough to minimize the contribution of the passive current when studying the initiation of a single pit. The composition of the SS was 18.9% Cr, 11.5% Ni, 1.8% Mo, 0.9% Si, the remainder being iron. A six-electrode cell was used allowing both the probe and the substrate to be polarized; a Faraday cage was used to minimize electrical interferences.

In the second approach (setup II), the SECM probe was replaced by a vertical glass microcapillary of 100 μm in inner diameter and 900 μm in outer diameter, produced with a laser puller (P-2000, Sutter Instrument) [9]. The top of the glass capillary was connected to a 100 μl Hamilton® syringe filled with a 2 M NaCl + 0.5 M of either H_2SO_4 or $HClO_4$ solution. A KD Scientific® syringe driver was used to gradually push the syringe piston at a linear velocity of 0.035 cm/s, giving a solution release rate of 10 μL/h. A 316L SS disk of 5 mm in diameter ($S = 0.2$ cm^2) was used as substrate in a conventional three electrode electrochemical cell (the experimental setup has already been described in details elsewhere [9]). The positioning of the probe above the centre of the substrate was achieved using electrolyte resistance measurements [8, 42]. In contrast with the Ag/AgCl microelectrode approach (setup I), using a syringe allows the chloride ion concentration in the close vicinity of the substrate to be controlled in long duration experiments (*i.e.* a few hours). This second device is thus a micro dispenser of a solution that can contain different ions at different solution and which can be used to locally modify the solution composition.

In all experiments, a large area platinum grid and a mercury/mercurous sulphate electrode (MSE) saturated in potassium sulphate were used as the counter-electrode and the reference electrode, respectively. All solutions were prepared with chemically pure chemicals (used as received) and twice-distilled deionized water.

2.2. Physical characterization

A Leica Stereoscan 440 scanning electron microscope (SEM) was used to image each obtained single pit and measure its radius. The pit depth was measured using a differential focusing technique with an optical microscope equipped with a micrometric screw. After the experiments, aliquots of electrolytic solutions were taken to quantify the amount of Fe, Ni, Cr, and Mo dissolved in the electrolyte. This was performed using an inductively coupled plasma optical emission spectrometer (ICP-OES) Perkin Elmer Optima 2000.

3. Results and discussion

The polarization curves of the 316L SS sample measured in both 0.5 M H_2SO_4 and 0.5 M $HClO_4$ solutions (data not shown) show a passive region that lies from about −0.4 V to 0.4 V/MSE. The passive current was low (about 300 nA) because of the small surface area, and there is no significant difference between the polarization curves obtained in both solutions.

3.1. Generation of a single pit using an AgCl probe (setup I).

The AgCl probe was precisely positioned above the centre of the 316L SS sample by measuring the electrolyte resistance between the probe and the reference electrode in two successive scans along the *x* and *y* axes, respectively. The probe was then moved vertically by performing an approach curve, and then, positioned at 10 μm above the steel substrate surface. Experimental details and typical recorded scans and approach curves are displayed in previous publications [9, 42].

It is well known that pitting occurs after localized attack by aggressive anions that break the passive film. In case of a highly resistive passive film, pitting often takes place in the vicinity of surface defects. To avoid such scenario and obtain reproducible pits at the center of the SS substrate, low resistive films were rigorously reproduced prior to each

experience. The native oxide film was first reduced by applying a potential of −0.8 V/MSE for 60 seconds. Then, a passive layer was formed by sweeping the sample potential to 0 V/MSE at a scan rate of 1 mV·s^{-1}. In a last step, the passive film was grown for 30 min after which the counter electrode was disconnected, allowing the sample to reach the open-circuit potential (OCP) of about 0.1 V/MSE. The Ag microelectrode was then biased at −0.8 V/MSE to release the Cl$^-$ anions from the AgCl deposit. In such configuration, the probe and the substrate formed a thin-layer cell similar to a tube, the dimensions of which are the probe diameter and the probe-to-substrate distance. Typical curves showing the evolution of the substrate OCP with Cl$^-$ concentration as a parameter in both 0.5 M H$_2$SO$_4$ and 0.5 M HClO$_4$ solutions are presented in Fig. 1a and 1b, respectively. Regardless the nature of the anion present in the electrolyte, the substrate potential, E_{316L}, dropped in the region of active metal dissolution (at about −0.75 V/MSE) within a few seconds after the Cl$^-$ release. SEM observations of the substrate at this stage did not exhibit any damaged surface, indicating that the Cl$^-$ anions alone were not able to initiate pitting at OCP (data not showed). The larger the amount of Cl$^-$ released, the longer the potential drop before recovering its initial value of about 0.1 V/MSE, which gives more evidence that the passive film was just momentarily stripped from the substrate after the Cl$^-$ release. By substituting ClO$_4^-$ for SO$_4^{2-}$, the substrate potential remains in the active domain markedly longer, which can be attributed to a difference in the adsorption strength of the anions either at the stripped surface or at the yet oxidized part of the 316L SS. This assumption is in agreement with literature as sulphate ions are known to better adsorb on metallic surfaces than perchlorate ions [43]. To force the pit initiation and propagation, the substrate must be biased to a more positive potential with respect to the active potential region. This is exemplified in Fig. 2: 12 seconds after the potential drop, the counter electrode was reconnected and at the same time, the substrate was biased at a potential of −0.1 V/MSE causing an immediate rise in the substrate current which

corresponds to the pit propagation. The current instantly reached a maximum value of about 2 mA in H_2SO_4 medium and then, decreased progressively till the complete repassivation after 1350 s. In contrast, in the $HClO_4$ solution, after pit initiation, the corrosion current magnitude decreased with strong oscillations before a sudden repassivation after 300 s, as shown in Fig. 3. Pitting propagation lasted 4 times longer in the H_2SO_4 solution than in the $HClO_4$ solution. At this potential of −0.1 V/MSE and for the same amount of SS dissolved ($Q_{HClO_4} = 87$ mC, $Q_{H_2SO_4} = 85$ mC), the pit mouth was circular in both cases, but the pit diameter was smaller (670 µm against 520 µm) and deeper (9 µm against 20 µm) in the $HClO_4$ solution, as shown on the optical micrographs presented in Fig. 4. In contrast with the well defined hemispherical pit shape obtained in H_2SO_4, a close examination of the picture presented in Fig. 4b shows concentric circles that were observed exclusively in presence of ClO_4^- anions and, therefore, were associated with the strong current oscillations observed in Fig. 3. It should be noted that our original experimental setup I allows the variations of the current to be ascribed undoubtedly to a single pit, and thus the concentric evolution of the active area to be linked to the measured current. There are several possibilities to explain why the nature of the non-aggressive anion influences the pitting behavior:

(i)   this might be due to a difference in the influence of SO_4^{2-} and ClO_4^- on the solubility of the metallic cations in the pit anolyte [3];

(ii)   this could be ascribed to the controversial role of SO_4^{2-} ions that are believed to participate to the formation of a $FeSO_4$ salt film when in contact with Fe^{2+} ions [8, 26];

(iii) this might also be related to a difference in the adsorption properties of the anions [17, 23].

The influence of the electrode potential on the pit propagation was investigated in the domain ranging from −0.4 to +0.4 V/MSE with potential steps of 100 mV. Increasing the potential can *a priori* have two opposite effects: it may increase the driving force of pit

propagation or promote the passive layer growth rate, and hence improves the resistance to metal dissolution. Fig. 5 reports the value of exchanged charge, Q_{316L}, involved in the SS dissolution as a function of the applied potential in both perchloric and sulfuric acid solutions. When identical experiments were performed, the dispersion of the results was lower always lower than 5%. For each experiment, the amount of chloride ion released was $Q_{AgCl} = 15$ mC. In presence of sulphate ions in the electrolyte, the higher the potential, the larger the amount of dissolved steel, with a quasi-linear relationship between Q_{316L} and E_{316L}, as shown in Fig. 5. In contrast, two different domains have been evidenced in the perchloric acid solution. Below -0.2 V/MSE, the exchanged charge increased with the potential, while it decreased at higher potentials, revealing the competition between the anodic dissolution reaction and the passivation of the bare metallic surface.

Anions are known to play an important role on the corrosion behavior of metals, essentially because of their adsorption properties since they may strongly adsorb on the metallic surfaces and modify the passive film formation. Bockris and co-workers [44] compared the adsorption of various anions (Cl^-, Br^-, ClO_4^-, SO_4^{2-} and OH^-) on several metallic surfaces by ellipsometry. Regardless of the nature of the investigated metal, the species showing the strongest adsorption is successively ClO_4^-, SO_4^{2-}, Cl^-, and Br^- when the increasing the potential. Our results are consistent with the previously proposed theory speculating that sulphates adsorb on steel surface and, as a consequence, poison pit repassivation in presence of chloride ions by forming metallic sulphate salts. In this context, the relative weak affinity of ClO_4^- with metals gives way to the resettlement of the passive film, which is known to grow faster with increasing applied potential [45].

Figs. 6a and 6b show the evolution of the pit diameter as well as the pit depth as function of the potential in H_2SO_4 and $HClO_4$, respectively. These measurements were performed using an optical microscope after the repassivation of the pit. When the

experiments were carried out in H_2SO_4 solution, the pit depth increased from about 3 μm to 30 μm when increasing the potential from -0.4 to +0.4 V/MSE while the pit diameter remained about constant over the whole potential range. Metal dissolution is clearly kinetically dependent on the polarization potential, which is characteristic of the metastable pit growth stage. Nevertheless, a close examination of Fig. 6a indicates that the pit depth notably increased with potential but then, levelled off at potentials higher than 0.1 V/MSE. This behaviour can be explained by the formation of a sulphate-iron rich salt layer at the bottom of the pit, which limits the dissolution kinetics. As a consequence, at potential higher than 0.1 V/MSE, the pit propagation is no longer under ohmic control.

In the $HClO_4$ solution, pits were larger and shallower, but it is difficult to draw conclusions on the influence of the applied potential because the exchanged charge during the pit dissolution is not a linear function of the potential, as shown in Fig. 5. However, pit repassivation is favored when increasing the potential and no evidence of the formation of a salt film in the bottom of the pit could have been evidenced.

Fig. 7 illustrates the evolution of the current provided by the dissolution of a single pit on 316L SS in 0.5 M $HClO_4$ as a function of the substrate potential. For clarity, only 4 current curves have been displayed to show that for potentials higher than −0.2 V/MSE, sharp current variations due to oscillations between active and passive state can be observed, which results in shortening the pit lifetime when increasing the potential. Comparison with results in sulfuric acid gives further evidence of the influence of sulphate ions on the repassivation mechanism in the high potential domain.

Fig. 8 compares the amount of the total dissolved species determined by ICP-OES analysis and that obtained using Faraday's law from the exchanged charge at a potential of -0.1 V/ MSE when assuming the dissolution of Fe, Cr, and Ni in Fe^{2+}, Cr^{3+}, and Ni^{2+} ions, respectively. The figure shows there was no selective dissolution whatever the non-aggressive

anion present in the media, since the nominal composition of the SS was obtained in both cases. The total amount of dissolved metallic compounds was found to be equal to the amount calculated with Faraday's law in the presence of ClO_4^- anions whereas about a quarter of the dissolved metallic cations were missing at all investigated potentials in the presence of SO_4^{2-} anions. This can be explained by the formation of a saturated metal salt film at the bottom of the pit due to the accumulation of corrosion products [14, 46-48]. It is believed that the metal-chloride or metal-sulphate salt layer is necessary to stabilise the pit propagation. In $HClO_4$, the fact that the whole amount of dissolved metal is retrieved in the electrolyte by ICP-OES and the oscillations of current during pit propagation, show that the salt layer has difficulties to settle and/or is rapidly dissolved. Pistorius and Burstein [3] have previously demonstrated that adding sulphate ions into the electrolyte reduced the stability product by lowering the solubility of the metal cations formed in the pit. There is no similar data in the literature for salt layers formed in the presence of perchlorate ions, but, considering solely ferrous salts, hydrated ferrous sulphate is known to be the least soluble product ($Ks_{25°C}$ ($FeSO_4$).$7H_2O$ = 3, $Ks_{20°C}$ ($Fe(ClO_4)_2$).$6H_2O$ = 70, $Ks_{20°C}$ ($FeCl_2.6H_2O$) = 90) [28, 49]. The presence of such hydrated ferrous sulphate permits revealing the reasons of both the relatively weak current values and the long-term pit propagation in H_2SO_4 compared to those observed in $HClO_4$. These results obtained for a single pit show that the counter ion can influence the pit propagation and the chemistry inside the pit: the film formation drastically changes the composition of the solution inside the pit, which plays a role on the stability of the pit.

3.2. Generation and sustainment of a single pit using a microcapillary (setup II).

In the previous experiments, the amount of Cl⁻ ions which could be released by the Ag/AgCl probe was limited by the amount of the AgCl deposited on the probe, roughly a few tens of mC. This amount was mainly used during the pit initiation, which could limit its

propagation. To overcome this difficulty and maintain a constant flux of Cl^- ions in the pit vicinity, the Ag/AgCl probe was replaced by a glass capillary linked to a 100 µl syringe containing a 2 M NaCl + 0.5 M of either H_2SO_4 or $HClO_4$ solution, which gave a 1000 fold increase of the amount of Cl^- available compared to setup I. In this configuration, the electrochemical cell formed a cylindrical thin-layer cell of radius of 900 µm and of thickness equal to 10 µm. The 316L SS sample underwent the same polishing procedure for the generation of a single pit using an AgCl probe. The capillary was positioned above the centre of the 316L disk, at a height of 10 µm, by measuring the electrolyte resistance between the SS substrate and the MSE during the glass capillary displacement. Injection of chloride ions in the cylindrical thin-layer cell below the capillary produced a single pit. The pits obtained at potentials up to 0 V/MSE were covered by perforated metallic layers, as confirmed by SEM observations (data not shown) in agreement with numerous previous studies that imaged the lacy cover formation pits using either video microscopy (2D) [20] or tomography studies (3D) [50]. Figs. 9a and 9b show the evolution of the current (in logarithmic scale) during the growth of a single pit in 0.5 M H_2SO_4 and 0.5 M $HClO_4$, respectively, at different potentials of the SS substrate. The pit dissolution rate increased markedly when the applied potential varied from -0.4 to 0.4 V/MSE in H_2SO_4 medium whereas pitting was inhibited in $HClO_4$ for 0.2 and 0.4 V/MSE, in agreement with the results obtained previously with the AgCl probe. Experiments carried out in H_2SO_4 medium reveal that the applied potential influences the morphology of the pits. Indeed, at low potentials, all pits were narrow, deep, and covered by a metallic layer while they were shallow, wide, and uncovered at above 0.2 V/MSE.

The effects of the applied potential upon pit growth are in agreement with those observed in Ernst and Newman's work on 304 SS foils of 50 µm thickness after 4 min in 1 M NaCl at 15 °C [21, 51], in which the pit width was found to increase markedly with increasing potential from 0.15 V to 0.3 V/MSE. The pit depth, however, was potential independent,

which is consistent with the existence of a highly electrical resistant salt film at the pit bottom [45, 46].

Fig. 10 compares the variations of current obtained during the 3-hour growth of single pits formed either at E_{316L} = 0 V/MSE, or at E_{316L} = 0 V/MSE followed by a potential step at 0.4 V/MSE in H_2SO_4, and at E_{316L} = 0 V/MSE in $HClO_4$. The current intensity reached a value of 3 mA in $HClO_4$ whereas it did not exceed 2 mA in H_2SO_4. In both solutions, the pits grew under a cover of lace metal and had identical diameter values (1.4 mm) after 3 hours, as shown in Figs. 11a and 11c. Pit depth values of 450 μm and 580 μm were obtained in H_2SO_4 and $HClO_4$, respectively. The corrosion rate at the pit bottom, which is diffusion controlled, is clearly slowed down by the presence of sulphate ions in the medium. When increasing the applied potential to 0.4 V/MSE while keeping the nature of the anion unchanged (SO_4^{2-}), the as-obtained pit was uncovered, or it lost its metal cover prior to be taken out of the electrolyte. At this potential, the pit diameter increased from 1.4 mm to 1.78 mm whereas its depth remained the same (Fig. 11). At this stage, it can be assumed that the potential rise increased solely the dissolution rate of the salt free lateral pit wall, as observed in Fig. 11b, giving more evidence to the establishment of a highly electrical resistant, saturated metal salt film at the bottom of the pit. This salt film hinders dissolution rate, converting the corrosion process from an activation-controlled process at the metal-electrolyte interface to a diffusion-controlled process inside the pit.

4. Conclusions

The influence of the nature of non-aggressive anions in the supporting electrolyte, and of the substrate potential, on the initiation and growth of single pits on 316L SS have been investigated using two different experimental setups. The initiation of the pit at the corrosion potential allows reproducible results to be obtained, in particular to investigate the influence of the SS potential on the pit propagation. The influence of the anion nature was significant:

pits initiated in sulphuric acid remained active longer than those obtained in perchloric acid. When sustained by a continuous injection of chloride ions, the single pit was shallower in sulphuric acid than in perchloric acid. From the ICP-OES analysis, the total amount of dissolved metallic components was found to be equal to the amount calculated with Faraday's law in the presence of ClO_4^- anions, whereas in the presence of SO_4^{2-} anions, about a quarter of the dissolved metallic cations were missing at all investigated potentials in the passive domain. The pitting dissolution rate of 316L SS increased markedly with the applied potential in H_2SO_4 medium. The presence of SO_4^{2-} inside the pit promotes the establishment of a metal salt film that decreases the dissolution rate after saturation, converting the process from an activation-controlled process at the metal-electrolyte interface to a diffusion-controlled process inside the pit. In contrast, pitting was inhibited in $HClO_4$ at potentials higher than 0 V/MSE. Indeed, in the presence of ClO_4^- ions, such salt film has difficulties to settle, giving way to a competition between the anodic dissolution reaction and the passivation of the bare metallic surface.

References

[1] G.T. Burstein, P.C. Pistorius, S.P. Mattin, The nucleation and growth of corrosion pits on stainless steel, Corros. Sci., 35 (1993) 57-62.

[2] G.T. Gaudet, W.T. Mo, T.A. Hatton, J.W. Tester, J. Tilly, H.S. Isaacs, R.C. Newman, Mass transfer and electrochemical kinetic interactions in localized pitting corrosion, AIChE J., 32 (1986) 949-958.

[3] P.C. Pistorius, G.T. Burstein, Growth of corrosion pits on stainless steel in chloride solution containing dilute sulfate, Corros. Sci., 33 (1992) 1885-1897.

[4] R. C. Alkire, K. P. Wong, The corrosion of single pits on stainless steel in acidic chloride solution, Corros. Sci., 28 (1988) 411-421.

[5] Maier, G. S. Frankel, Pitting Corrosion of Bare Stainless Steel 304 under Chloride Solution Droplets, J. Electrochem. Soc., 157 (2010) C302-C312.

[6] K. Fushimi, K. Azumi, M. Seo, Use of ion gun in liquid phase for local breakdown of passive film on iron, Proc. Electrochem. Soc., 98-17 (1999) 626-634.

[7] K. Fushimi, M. Seo, Initiation of a local breakdown of passive film on iron due to chloride ions generated by a liquid-phase ion gun, J. Electrochem. Soc., 148 (2001) B450-B456.

[8] N. Aouina, F. Balbaud-Celerier, F. Huet, S. Joiret, H. Perrot, F. Rouillard, V. Vivier, Single pit initiation on 316L austenitic stainless steel using scanning electrochemical microscopy, Electrochim. Acta, 56 (2011) 8589-8596.

[9] N. Aouina, F. Balbaud-Celerier, F. Huet, S. Joiret, H. Perrot, F. Rouillard, V. Vivier, A flow microdevice for studying the initiation and propagation of a single pit, Corros. Sci., 62 (2012) 1-4.

[10] N. J. Laycock, S. P. White, Computer simulation of single pit propagation in stainless steel under potentiostatic control, J. Electrochem. Soc., 148 (2001) B264-B275.

[11] H. S. Isaacs, A. J. Davenport, J. H. Cho, M. L. Rivers, S. R. Sutton, Application of in situ x-ray absorption and fluorescence measurements to analyze solutions in a simulated pit, Proc. Electrochem. Soc., 92-1 (1992) 354-363.

[12] H. S. Isaacs, J. H. Cho, A. J. Davenport, M. L. Rivers, S. R. Sutton, Application of in situ scanning X-ray fluorescence to study the concentration of metal ions in simulated pits, Corros.Control Low-Cost Reliab., Proc.- Int. Corros. Congr., 12th, 3B (1193) 1997-2004.

[13] T. Rayment, A. J. Davenport, A. J. Dent, J. P. Tinnes, R. J. K. Wiltshire, C. Martin, G. Clark, P. Quinn, J. F. Mosselmans, Characterisation of salt films on dissolving metal surfaces in artificial corrosion pits via in situ synchrotron x-ray diffraction, Electrochem. Commun. 10 (2008) 855-858.

[14] H. S. Isaacs, Behavior of resistive layers in the localized corrosion of stainless steel, J. Electrochem. Soc., 120 (1973) 1456-1462.

[15] H.P. Leckie, H.H. Uhlig, Environmental factors affecting the critical potential for pitting in 18-8 stainless steel, J. Electrochem. Soc., 113 (1966) 1262-1267.

[16] H.C. Man, D.R. Gabe, A study of pitting potentials for some austenitic stainless steels using a potentiodynamic technique, Corros. Sci., 21 (1981) 713-721.

[17] Y. Zuo, H. Wang, J. Zhao, J. Xiong, The effects of some anions on metastable pitting of 316L stainless steel, Corros. Sci., 44 (2001) 13-24.

[18] W. Schwenk, Theory of stainless steel pitting, Corrosion (Houston, TX, U.S.), 20 (1964) 129t-137t.

[19] I.L. Rosenfeld, I.S. Danilov, Electrochemical aspects of pitting corrosion, Corros. Sci., 7 (1967) 129-142.

[20] Y. Kolotyrkin, Pitting corrosion of metals, Corrosion (Houston, TX, U.S.), 19 (1963) 261t-268t.

[21] P. Ernst, R.C. Newman, Pit growth studies in stainless steel foils. I. Introduction and pit growth kinetics, Corros. Sci., 44 (2002) 927-941.

[22] I. Rosenfeld, W. Maximtschuk, Z. Physik. Chem., 215 (1960) 25.

[23] T. Hong, M. Nagumo, The effect of SO_4^{2-} concentration in NaCl solution on the early stages of pitting corrosion of type 430 stainless steel, Corros. Sci., 39 (1997) 961-967.

[24] M.H. Moayed, R.C. Newman, Aggressive effects of pitting "inhibitors" on highly alloyed stainless steels, Corros. Sci., 40 (1998) 519-522.

[25] M.H. Moayed, R.C. Newman, Deterioration in critical pitting temperature of 904L stainless steel by addition of sulfate ions, Corros. Sci., 48 (2006) 3513-3530.

[26] R.C. Alkire, K.P. Wong, The corrosion of single pits on stainless steel in acidic chloride solution, Corros. Sci., 28 (1988) 411-421.

[27] K.J. Vetter, H.H. Strehblow, Pitting corrosion in an early stage and its theoretical implications, Int. Corros. Conf. Ser., NACE-3 (1974) 240-251.

[28] H.W. Pickering, R.P. Frankenthal, Mechanism of localized corrosion of iron and stainless steel. I. Electrochemical studies, J. Electrochem. Soc., 119 (1972) 1297-1304.

[29] H.W. Pickering, R.P. Frankenthal, On the Mechanism of Localized Corrosion of Iron and Stainless Steel. Morphological Studies J. Electrochem. Soc, 119 (1972) 1304-1310.

[30] T. Laitinen, Localized corrosion of stainless steel in chloride, sulfate and thiosulfate containing environments, Corros. Sci., 42 (2000) 421-441.

[31] C. Gabrielli, S. Joiret, M. Keddam, N. Portail, P. Rousseau, V. Vivier, Single pit on iron generated by SECM, Electrochim. Acta, 53 (2008) 7539-7548.

[32] C. Gabrielli, S. Joiret, M. Keddam, H. Perrot, N. Portail, P. Rousseau, V. Vivier, Development of a Coupled SECM-EQCM Technique for the Study of Pitting Corrosion on Iron, J. Electrochem. Soc., 153 (2006) B68-B74.

[33] C. Gabrielli, S. Joiret, M. Keddam, H. Perrot, N. Portail, P. Rousseau, V. Vivier, A SECM assisted EQCM study of iron pitting, Electrochim. Acta, 52 (2007) 7706-7714.

[34] Y. Gonzalez-Garcia, G.T. Burstein, S. Gonzalez, R.M. Souto, Imaging metastable pits on austenitic stainless steel in situ at the open-circuit corrosion potential, Electrochem. Commun., 6 (2004) 637-642.

[35] J.J. Santana, J. Gonzalez-Guzman, L. Fernandez-Merida, S. Gonzalez, R.M. Souto, Visualization of local degradation processes in coated metals by means of scanning electrochemical microscopy in the redox competition mode, Electrochim. Acta, 55 (2010) 4488-4494.

[36] M.B. Jensen, D.E. Tallman, Application of SECM to corrosion studies, Electroanal. Chem., 24 (2012) 171-286.

[37] A.M. Simoes, D. Battocchi, D.E. Tallman, G.P. Bierwagen, SVET and SECM imaging of cathodic protection of aluminium by a Mg-rich coating, Corros. Sci., 49 (2007) 3838-3849.

[38] T.E. Lister, P.J. Pinhero, The effect of localized electric fields on the detection of dissolved sulfur species from Type 304 stainless steel using scanning electrochemical microscopy, Electrochim. Acta, 48 (2003) 2371-2378.

[39] C.G. da Silva, I.C.P. Margarit-Mattos, O.R. Mattos, H. Perrot, B. Tribollet, V. Vivier, The molybdate-zinc conversion process, Corros. Sci., 51 (2009) 151-158.

[40] D. Sidane, O. Devos, M. Puiggali, M. Touzet, B. Tribollet, V. Vivier, Electrochemical characterization of a mechanically stressed passive layer, Electrochem. Commun., 13 (2011) 1361-1364.

[41] K. Fushimi, K. Azumi, M. Seo, Use of a liquid-phase ion gun for local breakdown of the passive film on iron, J. Electrochem. Soc., 147 (2000) 552-557.

[42] H. Bouazaze, J. Fransaer, F. Huet, P. Rousseau, V. Vivier, Electrolyte-resistance change due to an insulating sphere in contact with a disk electrode, Electrochim. Acta, 55 (2010) 1645-1655.

[43] D. Landolt, Corrosion and surface chemistry of metals, EPFL Press Lausane, CRC Taylor and Francis, Boca Raton, FL 33487, 2007.

[44] J.O.M. Bockris, W.K. Paik, M.A. Genshaw, Adsorption of anions at the solid-solution interface. Ellipsometric study, J. Phys. Chem., 74 (1970) 4266-4275.

[45] S. Haupt, H.H. Strehblow, A combined surface analytical and electrochemical study of the formation of passive layers on Fe/Cr alloys in 0.5 M H2SO4, Corros. Sci., 37 (1995) 43-54.

[46] T.R. Beck, R.C. Alkire, Occurrence of salt films during initiation and growth of corrosion pits, J. Electrochem. Soc., 126 (1979) 1662-1666.

[47] J.W. Tester, H.S. Isaacs, Diffusional effects in simulated localized corrosion, J. Electrochem. Soc., 122 (1975) 1438-1445.

[48] H.S. Isaacs, J.H. Cho, M.L. Rivers, S.R. Sutton, In situ x-ray microprobe study of salt layers during anodic dissolution of stainless steel in chloride solution, J. Electrochem. Soc., 142 (1995) 1111-1118.

[49] W.F. Linke, Solubilities of Inorganic and Metal-Organic Compounds, 4th ed. Van Nostrand, Princeton, NJ, Vol. 1, 1958.

[50] S. M. Ghahari, A. J. Davenport, T. Rayment, T. Suter, J. P. Tinnes, C. Padovani, J. A. Hammons, M. Stampanoni, F. Marone, R. Mokso, In situ synchrotron X-ray micro-tomography study of pitting corrosion in stainless steel, Corros. Sci., 53 (2011) 2684-2687.

[51] P. Ernst, R.C. Newman, Pit growth studies in stainless steel foils. II. Effect of temperature, chloride concentration and sulphate addition, Corros. Sci., 44 (2002) 943-954.
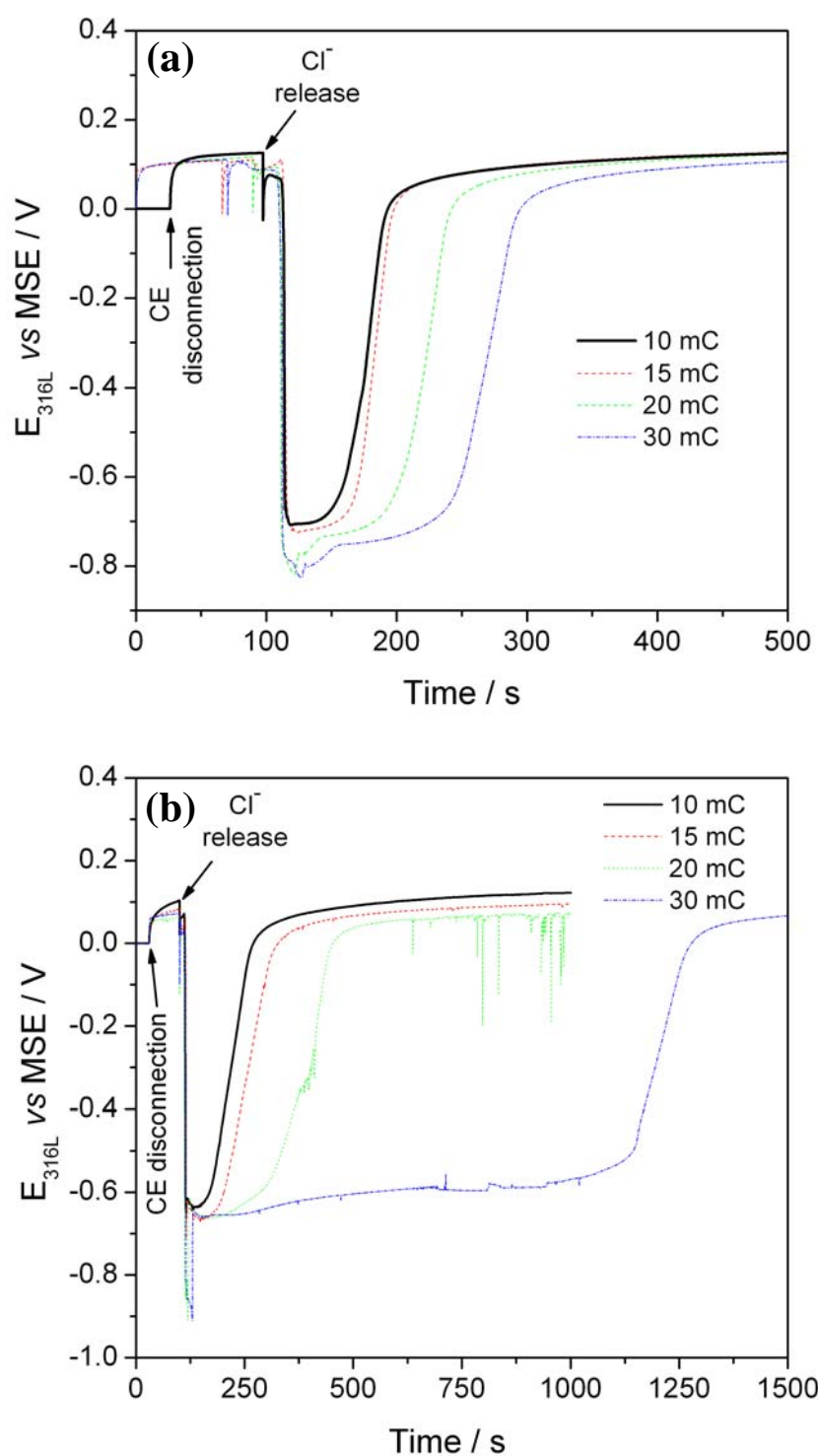
Figure Captions

Fig. 1. Evolution of the open circuit potential of the SS substrate with Cl⁻ concentration as a parameter in 0.5 M H_2SO_4 (a) and 0.5 M $HClO_4$ (b). Q_{AgCl} = 10 mC (black line), 15 mC (red line), 20 mC (green line), and 30 mC (blue line). Tip-to-substrate distance z = 10 μm.
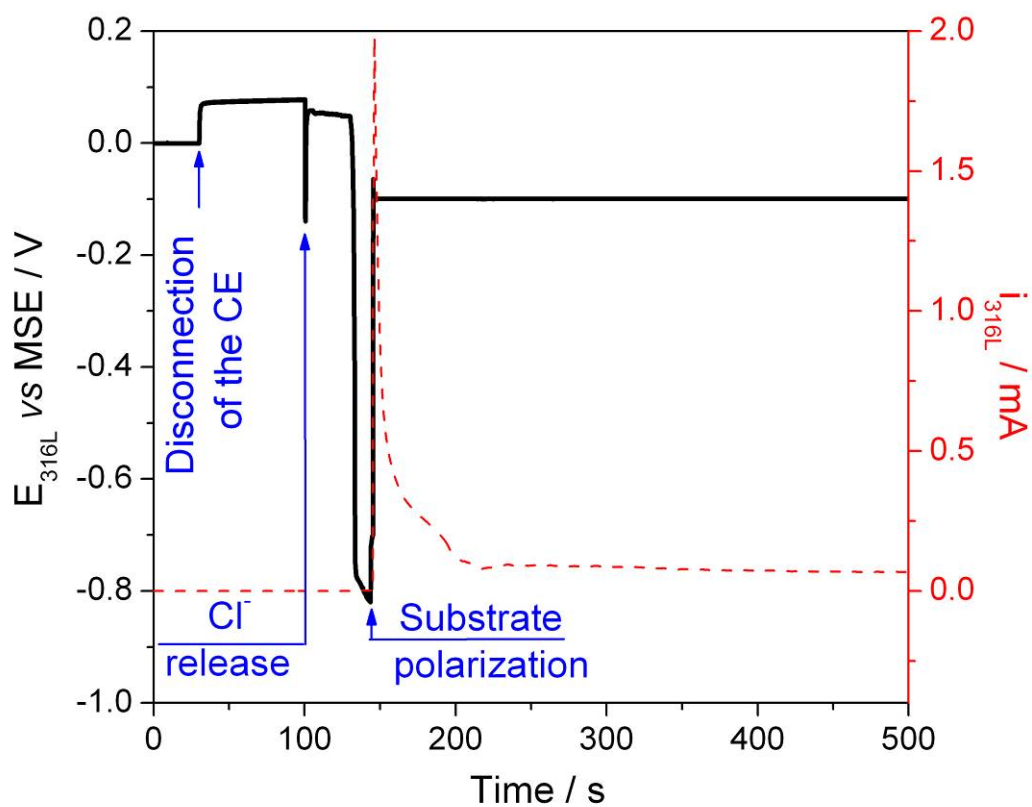
Fig. 2. Evolution of the substrate potential (black solid line, left ordinate) and current (red dashed line, right ordinate) for a single pit obtained on a 316L SS in 0.5 M H_2SO_4 – tip-to-substrate distance z = 10 μm and Q_{AgCl} = 15 mC.
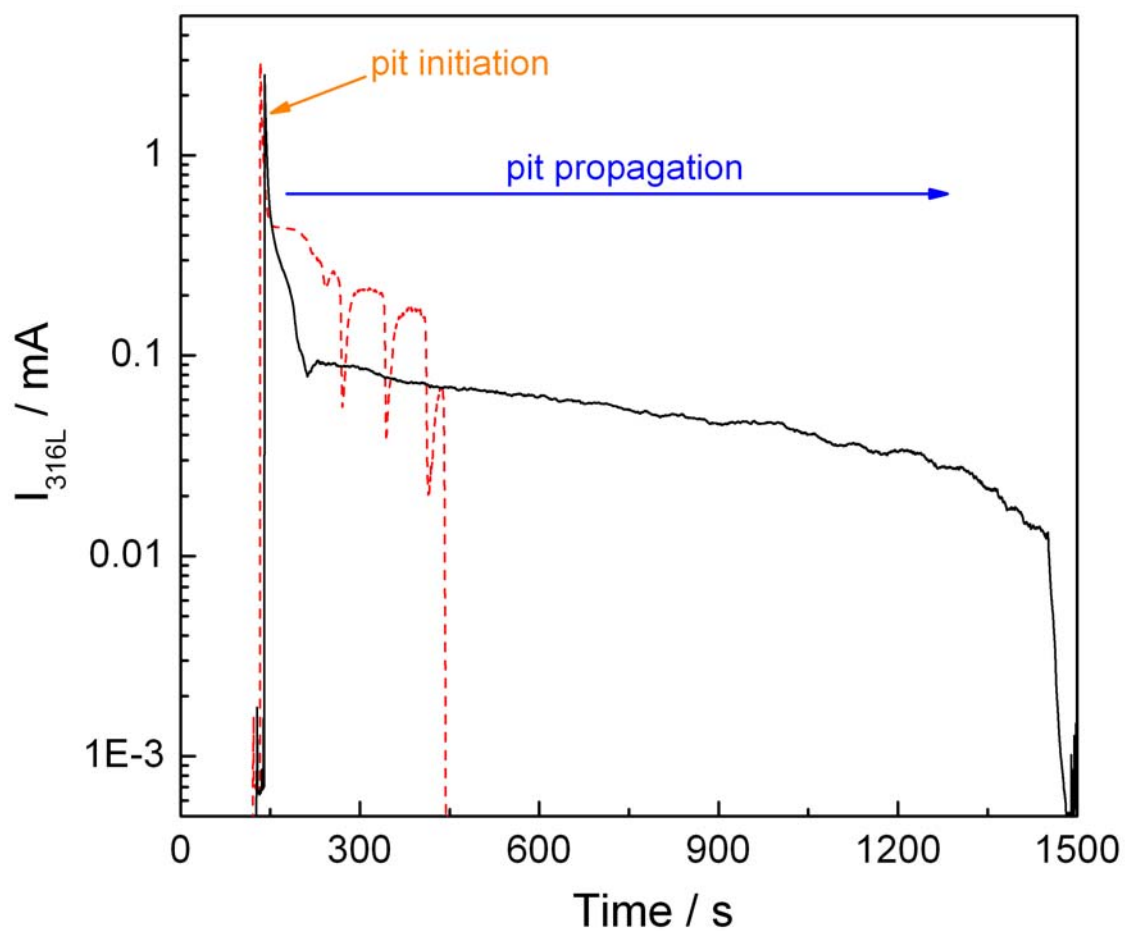
Fig. 3. Evolution of the current generated by a single pit on 316L SS in 0.5 M H_2SO_4 (black solid line) and 0.5 M $HClO_4$ (red dashed line). E_{316L}= −0.1 V/MSE, tip-to-substrate distance z = 10 μm and Q_{AgCl} = 15 mC.

Fig. 4. Optical micrographs of pits generated on 316L SS in 0.5 M H_2SO_4 (a) and 0.5 M $HClO_4$ (b). E_{316L}= −0.1 V/MSE, tip-to-substrate distance z = 10 μm and Q_{AgCl} = 15 mC.

Fig. 5. Exchanged charge during the single pit dissolution as a function of the applied potential on 316L SS in 0.5 M H_2SO_4 (black circles) and 0.5 M $HClO_4$ (red squares). Tip-to-substrate distance z = 10 μm and Q_{AgCl} = 15 mC.

Fig. 6. Measured pit depth (black circles) and diameters (red squares) as a function of the applied potential for pits obtained on 316L SS in 0.5 M H_2SO_4 (a) and 0.5 M $HClO_4$ (b). Tip-to-substrate distance z = 10 μm and Q_{AgCl} = 15 mC.

Fig. 7. Evolution of the current generated by a single pit on 316L SS in 0.5 M $HClO_4$ with the substrate potential as a parameter. Tip-to-substrate distance z = 10 μm and Q_{AgCl} = 15 mC.

Fig. 8. Number of moles of dissolved species determined by ICP-OES analysis in $HClO_4$ and H_2SO_4 solutions. The volume of the electrolytic solution was 50 cm³, E_{316L} = −0.1 V/MSE, tip-to-substrate distance z = 10 μm and Q_{AgCl} = 15 mC.

Fig. 9. Evolution of the current generated by a single pit on 316L SS in 0.5 M H_2SO_4 (a) and 0.5 M $HClO_4$ (b). at different substrate potential. Tip-to-substrate distance $z = 10$ μm, flow rate of the chloride solution in the microcapillary: 10 μL/h.

Fig. 10. Evolution of the current generated by a single pit at 0 V/MSE on 316L SS in 0.5 M $HClO_4$ and 0.5 M H_2SO_4. The dotted line indicates a potential step from 0 to 0.4 V/MSE. Tip-to-substrate distance $z = 10$ μm, flow rate of the chloride solution in the microcapillary: 10 μL/h.

Fig. 11. SEM observations of a single pit generated on 316L SS in 0.5 M H_2SO_4 at $E_{316L} = 0$ V/MSE (a) 0 and 0.4 V/MSE (c) and in 0.5 M $HClO_4$ at $E_{316L} = 0$ V/MSE (b) (same experiments as in Fig. 15).

Fig. 1. Evolution of the open circuit potential of the SS substrate with Cl$^-$ concentration as a parameter in 0.5 M H$_2$SO$_4$ (a) and 0.5 M HClO$_4$ (b). Q_{AgCl} = 10 mC (black line), 15 mC (red line), 20 mC (green line), and 30 mC (blue line). Tip-to-substrate distance z = 10 μm.

Fig. 2. Evolution of the substrate potential (black solid line, left ordinate) and current (red dashed line, right ordinate) for a single pit obtained on a 316L SS in 0.5 M H_2SO_4 – tip-to-substrate distance $z = 10$ μm and $Q_{AgCl} = 15$ mC.

Fig. 3. Evolution of the current generated by a single pit on 316L SS in 0.5 M H_2SO_4 (black solid line) and 0.5 M $HClO_4$ (red dashed line). $E_{316L}= -0.1$ V/MSE, tip-to-substrate distance z = 10 μm and Q_{AgCl} = 15 mC.

Fig. 4: Optical micrographs of pits generated on 316L SS in 0.5 M H_2SO_4 (a) and 0.5 M $HClO_4$ (b). $E_{316L} = -0.1$ V/MSE, tip-to-substrate distance $z = 10$ μm and $Q_{AgCl} = 15$ mC.

Fig. 5. Exchanged charge during the single pit dissolution as a function of the applied potential on 316L SS in 0.5 M H_2SO_4 (black circles) and 0.5 M $HClO_4$ (red squares). Tip-to-substrate distance $z = 10$ μm and $Q_{AgCl} = 15$ mC.

Fig. 6. Measured pit depth (black circles) and diameters (red squares) as a function of the applied potential for pits obtained on 316L SS in 0.5 M H_2SO_4 (a) and 0.5 M $HClO_4$ (b). Tip-to-substrate distance $z = 10$ μm and $Q_{AgCl} = 15$ mC.

Fig. 7. Evolution of the current generated by a single pit on 316L SS in 0.5 M HClO$_4$ with the substrate potential as a parameter. Tip-to-substrate distance z = 10 μm and Q_{AgCl} = 15 mC.
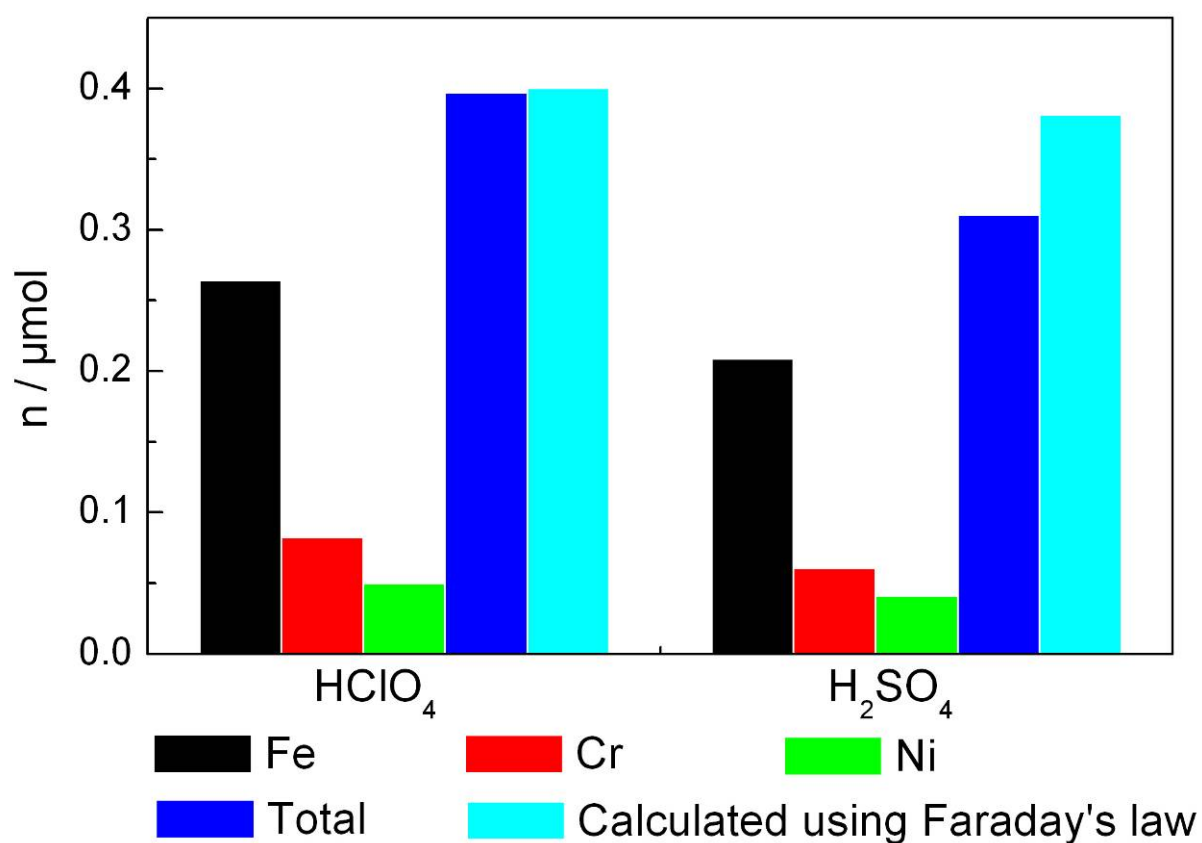
Fig. 8. Number of moles of dissolved species determined by ICP-OES analysis in $HClO_4$ and H_2SO_4 solutions. The volume of the electrolytic solution was 50 cm^3, E_{316L} = −0.1 V/MSE, tip-to-substrate distance z = 10 μm and Q_{AgCl} = 15 mC.
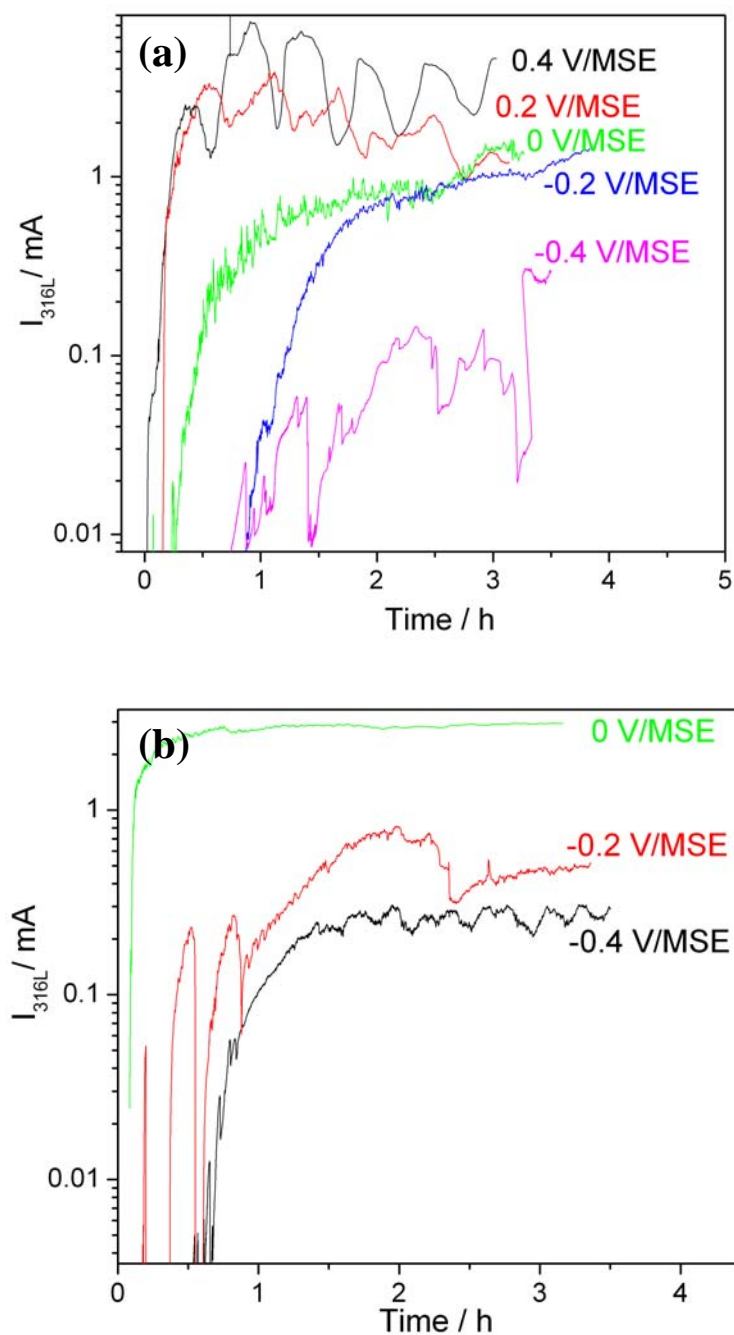
Fig. 9. Evolution of the current generated by a single pit on 316L SS in 0.5 M H_2SO_4 (a) and 0.5 M $HClO_4$ (b). at different substrate potential. Tip-to-substrate distance $z = 10$ μm, flow rate of the chloride solution in the microcapillary: 10 μL/h.
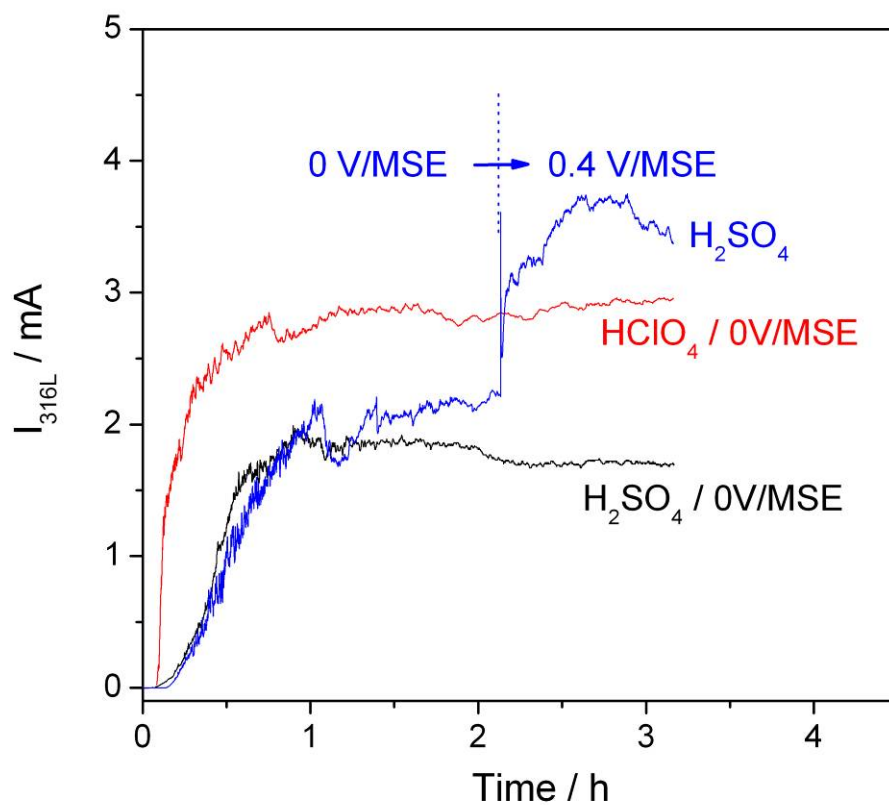
Fig. 10. Evolution of the current generated by a single pit at 0 V/MSE on 316L SS in 0.5 M HClO₄ and 0.5 M H₂SO₄. The dotted line indicates a potential step from 0 to 0.4 V/MSE. Tip-to-substrate distance z = 10 µm, flow rate of the chloride solution in the microcapillary: 10 µL/h.
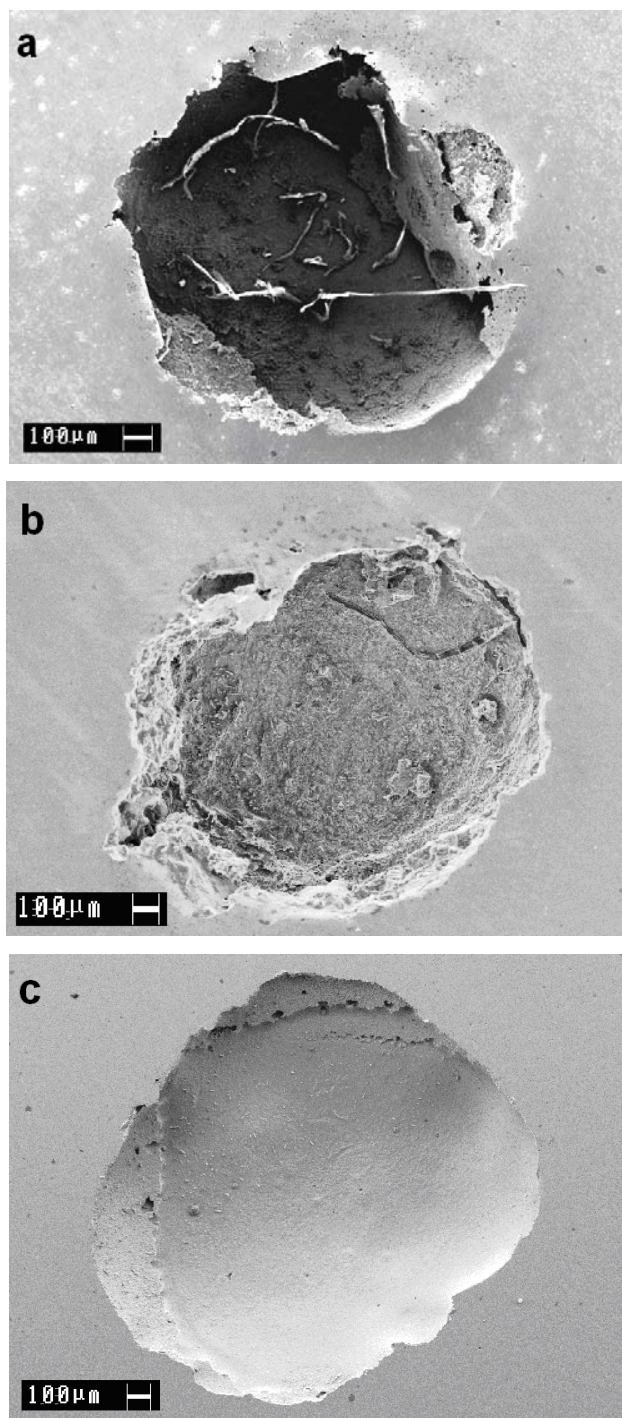
Fig. 11: SEM observations of a single pit generated on 316L SS in 0.5 M H_2SO_4 at $E_{316L} = 0$ V/MSE (a) 0 and 0.4 V/MSE (c) and in 0.5 M $HClO_4$ at $E_{316L} = 0$ V/MSE (b) (same experiments as in Fig. 15).